Electron scattering spectroscopy by a high magnetic field in quantum cascade lasers

A. Leuliet,[1,2] A. Vasanelli,[1,2,*] A. Wade,[3] G. Fedorov,[3] D. Smirnov,[3] G. Bastard,[4] and C. Sirtori[1,2]
[1]*Laboratoire "Matériaux et Phénomènes Quantiques," Université Denis Diderot Paris VII, 75005 Paris, France*
[2]*Thales Research and Technology, 91767 Palaiseau Cedex, France*
[3]*National High Magnetic Field Laboratory, Tallahassee, Florida 32310, USA*
[4]*Laboratoire Pierre Aigrain, Ecole Normale Supérieure, 75005 Paris, France*
(Received 8 September 2005; revised manuscript received 22 December 2005; published 10 February 2006)

We present a detailed experimental and theoretical study of a GaAs/AlGaAs mid-infrared quantum cascade laser (QCL) under a strong magnetic field. The emitted power and the magnetoresistance show strong oscillations as a function of B, due to a magnetic field modulation of the lifetime of the upper state of the laser transition. The analysis of these oscillations shows a modulation of the electron lifetime due to inelastic (LO-phonon emission) and elastic scattering mechanisms. We show that at low temperature, the interface roughness scattering is the most efficient elastic relaxation mechanism; it becomes dominant whenever LO-phonon emission is inhibited by the magnetic field. By comparing experimental and theoretical results, we are able to estimate the relative weight of elastic and inelastic scattering. The magnetic field is thus a powerful spectroscopic tool to study the scattering mechanisms in QCL active regions.

DOI: 10.1103/PhysRevB.73.085311 PACS number(s): 63.22.+m, 72.10.−d, 85.60.Bt

I. INTRODUCTION

The application of an intense magnetic field along the growth direction of a semiconductor quantum well breaks the two-dimensional (2D) in-plane continuum into discrete Landau levels. As a consequence, the lifetime of an electron in an excited state is strongly modified and modulated by the magnetic field. This general property of heterostructures has recently been exploited in mid-infrared and far-infrared quantum cascade lasers.[1–4] In mid-infrared lasers, Landau quantization was exploited in order to control electron-LO-phonon scattering.[1–3] In the THz range, the enhancement of the intersubband emission[4] and then of the laser intensity[5] has been observed. Furthermore, the quenching of nonradiative relaxation channels for some values of the magnetic field is responsible for a drastic reduction of the threshold current density, as observed by many groups.[5–8]

The aim of this work is to use magnetic fields as a spectroscopic tool to study the scattering mechanisms that take place in a mid-infrared quantum cascade laser (QCL). In a previous paper,[2] we showed that the application of a strong magnetic field along the current direction of this device causes oscillations in the laser emission intensity. We attributed this effect to a variation of the optical gain engendered by a change of the lifetime of the upper state of the laser transition. In this paper, we calculate this lifetime, showing that oscillations are mostly due to a magnetic field modulation of the lifetime through an inelastic scattering mechanism (LO-phonon) and an elastic one (interface roughness). As a consequence, we can estimate the relative weight of elastic and inelastic diffusion in the active region of a mid-infrared QCL at $B=0$.

By studying low temperature magnetoresistance of mid-infrared QCLs Smirnov *et al.*[3] showed that the relaxation rate via acoustic phonons (quasielastic scattering mechanism) is almost an order of magnitude smaller than via LO phonons. Similar results were also obtained by Radovanović *et al.*[9] in a recent paper. These authors calculated population densities and optical gain as a function of the magnetic field for the mid-infrared QCL of Ref. 2. In the present work, we will show that interface roughness is also a very efficient scattering mechanism, which strongly affects optical and transport properties.

The role of disorder on the luminescence spectra of a QCL in a strong magnetic field has only been studied in the case of a magnetic field parallel to the layers.[10] Interface roughness and ionized impurity scattering were taken into account to interpret the experimental data of Blaser *et al.*[11] on a QCL based on a photon assisted tunneling transition. In this case, the disorder potential causes a rapid decrease of the luminescence peak and tends to cancel its expected redshift.

In this paper, we present a detailed experimental and theoretical study of a GaAs/AlGaAs QCL which emits at 11 μm and is subjected to a strong magnetic field applied along the growth direction. Through comparison between experimental and modeling results, we elucidate the role of interface roughness scattering in the relaxation of electrons in the active region.

In Sec. II, we present the laser structure and the experimental setup. In Sec. III, we present the experimental results of the emitted power and measured voltage as a function of B at constant injection current.

Section IV is devoted to the theoretical model. We first apply to the actual QCL structure our model of LO-phonon scattering rate calculations in the presence of the magnetic field. We show that in order to reproduce the measured emitted power as a function of B, we have to introduce an elastic scattering mechanism in our model. The contribution of different elastic or quasielastic mechanisms is then calculated, showing that the interface roughness is the dominant effect in our structure.

In Sec. V, we analyze transport measurements below and above threshold. We show that below the threshold, the oscillations of $V(B)$ are directly related to the oscillations of the scattering time. On the contrary, above threshold there is an

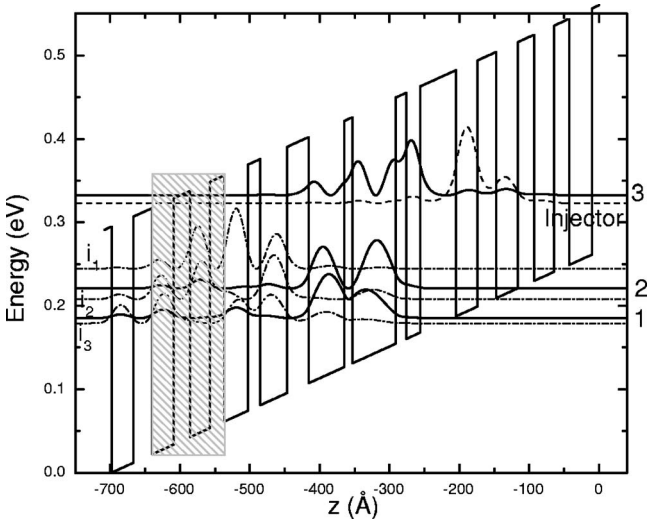

FIG. 1. Conduction band diagram of the active region. The shaded zone represents the doped region.

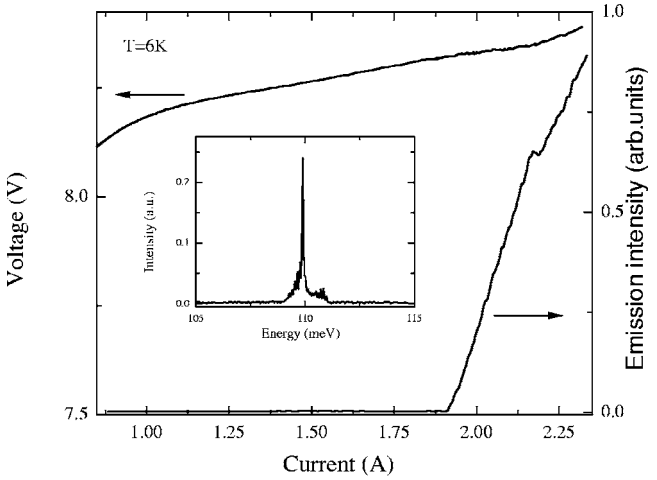

FIG. 2. $P(I)$ and $I(V)$ curves measured at 6 K and $B=0$. Inset: Laser emission spectrum.

important contribution of the stimulated emission lifetime, which primarily controls the lifetime of the upper state.

Finally, in Sec. VI, we conclude and discuss possible perspectives of the present work.

II. EXPERIMENT

We studied $GaAs/Al_{0.33}Ga_{0.67}As$ QCLs emitting at a wavelength of 11.3 μm. The structure was grown on a GaAs substrate using molecular beam epitaxy. It consists of 40 identical periods connected in a series. Each period includes an active region responsible for light emission and superlattice emitter-collector regions. The active region of the laser structure is shown in Fig. 1 and is described in detail elsewhere.[12] The active zone is essentially a three level laser system. Electrons are electrically injected into the third level. The laser transition takes place between levels indicated by 3 and 2, while level 1, engineered such that E_2-E_1 is approximately equal to the LO-phonon energy, helps the fast depopulation of level 2 to maintain population inversion between levels 3 and 2. In the figure, we also indicate by i_1, i_2, and i_3 some of the injector states which propagate into the active region.

The structures are processed into mesa-etched bars 20 μm wide and 1 mm long. The devices are In soldered ridge side up on gold coated alumina substrates, wire bonded, and mounted on a brass heat sink. The QCL sample is then mounted in a helium cryostat and placed at the center of DC magnets capable of a maximum field of 18 T (superconducting solenoid), 25–33 T (resisitive magnets), or 45 T (hybrid magnet), such that the magnetic field lines are perpendicular to the QW planes and parallel to the current flow direction: $\vec{I} \| \vec{B}$. All measurements were performed at 6 K and in a pulsed current mode. Current pulses of 0.4–2 μs pulse width and at 1–2 kHz repetition frequency are injected into the QCL sample through a low-impedance transmission line or a semirigid coax cable. The emitted light is reflected up a brass light pipe and guided toward an external liquid nitrogen cooled HgCdTe detector. To acquire the light versus magnetic field $P(B)$ or voltage versus magnetic field $V(B)$ curves, constant current pulses are applied to the QCL sample and the signals are measured while sweeping the field. To measure the magnetic field dependence of $P(I)$ and $I(V)$ curves, the current pulse amplitudes are linearly modulated at a frequency of 0.05 Hz while the magnetic field is swept at a very slow rate of 0.2 T/min.

III. EXPERIMENTAL RESULTS

At liquid helium temperature, the QCL exhibits laser action with a threshold current I_{th} of 1.95 A. In the following text, we normalize all the currents to this value. The light-current and voltage-current characteristics of the sample at zero magnetic field are shown in Fig. 2. The insert on this figure shows the emission spectrum of the QCL under study. The peak power is obtained at the wavelength of 11.3 μm that corresponds to approximately 110 meV.

Laser emission shows strong oscillations as a function of the magnetic field as reported in Fig. 3. In this configuration, the laser threshold is also an oscillatory function of a magnetic field as indicated in Fig. 3. The threshold current is reduced by a factor of 2 at $B \approx 33$ T [as shown in Fig. 4(a)], where the maximum emission intensity occurs, while at $B \approx 26$ T and at $B > 38$ T the emission is completely suppressed.

Similar, but less pronounced oscillations are found on the $V(B)$ curves measured during the same field sweeps at constant current [Fig. 4(b)]. The inset of this figure presents the oscillating part of the measured voltage (obtained by the subtraction of the monotonous part of the magnetoresistance) as a function of the magnetic field. It is apparent that these oscillations are more pronounced at current values below the threshold, i.e., without the laser radiation in the cavity. This behavior will be discussed in Sec. V.

IV. MODEL

A. Energy level calculation

Energy levels and wave functions are calculated by using a two-band Kane model.[13] When a magnetic field B is ap-

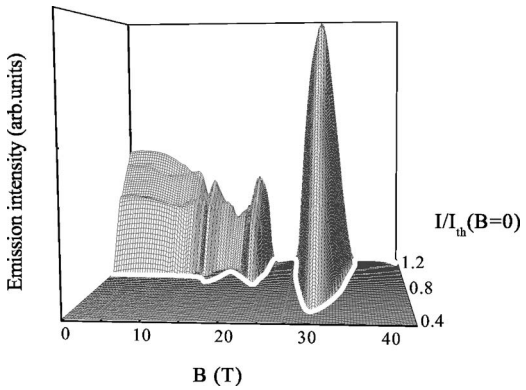

FIG. 3. Emission intensity of GaAs/AlGaAs QCL as a function of the current bias (normalized to the threshold current value) and the magnetic field. The white solid line indicates QCL current threshold. $T=6$ K.

plied along the growth direction of the structure, the different subbands split into discrete energy levels (Landau levels), given by

$$\varepsilon_{n,p} = E_n + \left(p + \frac{1}{2}\right)\hbar\omega_c, \tag{1}$$

where n and p are integers, $\hbar\omega_c = \hbar eB/m^*(\varepsilon_{n,p})$ is the cyclotron energy, and E_n the energies of the subband edges at $B=0$. The energy-dependent effective mass $m^*(\varepsilon_{n,p})$ is calculated within the Kane model.[13] We checked the effect of band nonparabolicity by comparing our results to those obtained by an expansion[14] up to the fourth order in k for the active region shown in Fig. 1. The two approaches are equivalent for the ground $p=0$ Landau level of the subbands $n=1$, 2, 3 up to 40 T. A slight discrepancy (a few percent) is found for excited Landau levels at large B values ($B>30$ T), when higher orders in the k expansion are needed in the model of Ref. 14.

B. LO-phonon scattering and magnetophonon resonances

The electron-LO-phonon scattering rates versus the magnetic field were recently calculated by Becker *et al.*[15] In this model, the overall optical response of the sample originates from a huge collection of similar ideal μ samples which differ from each other because the well width L varies in a random fashion from one μ sample to the other.[16] The thickness variation from a terrasse to the other is thus responsible for an inhomogeneous broadening of Landau levels, characterized by a parameter δ. In the following, we use this model to quantitatively explain the oscillations in the emitted power of the QCL discussed in Sec. III.

The oscillating behavior of the emitted power has already been studied in previous papers:[1,2] the laser intensity has minima whenever an electron on the $|3,0\rangle$ level can relax on the $|2,p\rangle$ or $|1,p\rangle (p>0)$ Landau levels by emitting one LO phonon. This situation takes place whenever the following condition is fulfilled (magnetophonon resonance):

$$E_3 - E_n - p\hbar eB/m^*(\varepsilon_{n,p}) - \hbar\omega_{LO} = 0. \tag{2}$$

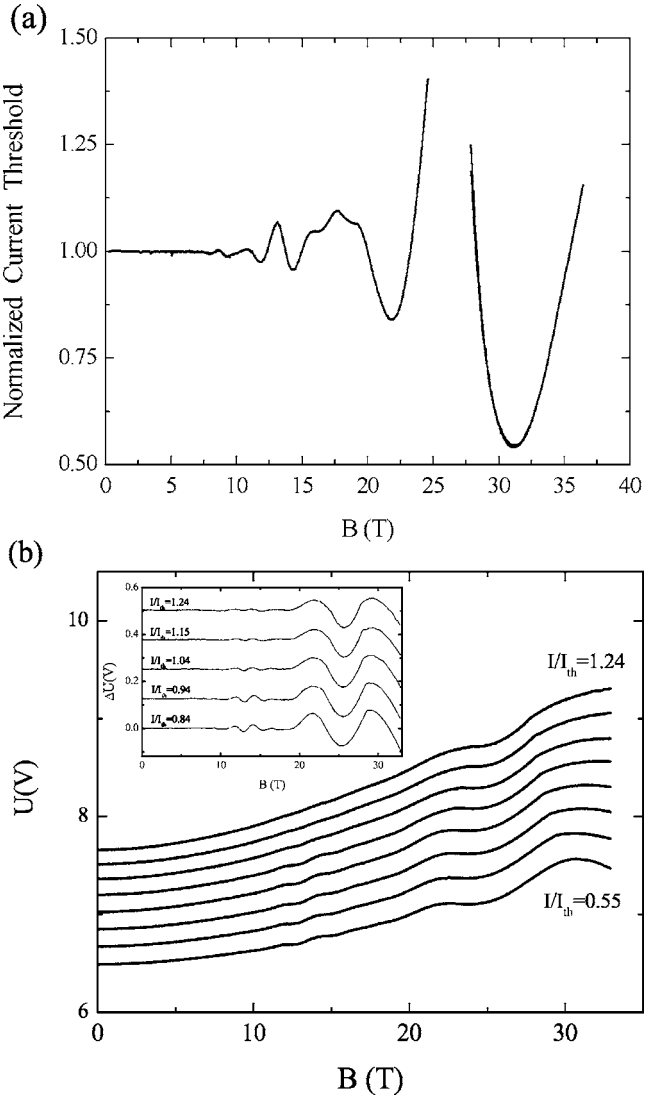

FIG. 4. (a) Density current threshold normalized to J_{th} at $B=0$ T as a function of the magnetic field. (b) Voltage across the QCL as a function of the magnetic field at different currents ($I/I_{th}=0.55$, 0.64, 0.74, 0.84, 0.94, 1.04, 1.15, 1.24) and $T=6$ K. Inset: Oscillatory component of the measured voltage near the current threshold at $B=0$ T.

Figure 5(a) shows the calculated Landau levels versus B for the three subbands of the active region. The dashed line represents the energy $\varepsilon_{3,0}-\hbar\omega_{LO}$, as a guide for the eye to evidence magnetophonon resonances (two of them are indicated with a circle).[17]

In order to reproduce the measured oscillations of the emitted power, a simplified system of QCL rate equations is used[18]

$$\dot{n}_3 = \eta\frac{J}{q} - \frac{n_3}{\tau_3} - \sigma_0 S n_3,$$

$$\dot{S} = \sigma_0 S n_3 - \tilde{c}\alpha S, \tag{3}$$

where S is the areal density of photons, η is the injection efficiency, J is the injected current density, n_3 is the areal

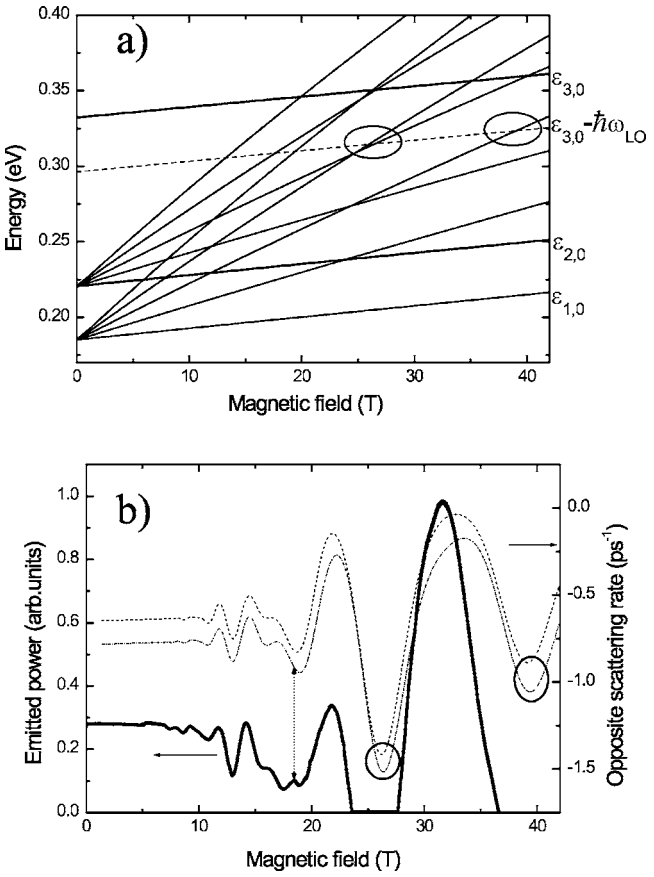

FIG. 5. (a) Landau levels as a function of the magnetic field. The circles indicate magnetophonon resonances. (b) Emitted power measured at the current $I=1.42$ A (solid line) compared to $-1/\tau_3$ as a function of the magnetic field. The dashed line is calculated by taking into account only relaxation to $|2,p\rangle$ and $|1,p\rangle$ Landau levels; the dashed-dotted line also includes contributions from i_1, i_2, i_3 states (see Fig. 1).

concentration of electrons on subband 3, σ_0 is the cross section per unit of time, $\tilde{c}$ is the velocity of light in vacuum divided by the mode refractive index, and α is the losses. We suppose that the subband 2 depopulation is very fast and thus that the population of level 2 can be neglected. By solving the system, Eq. (3), in the stationary state, we find either $S=0$ and $\eta(J/q)=n_3/\tau_3$ or

$$S=\frac{\eta}{\alpha\tilde{c}}\frac{J}{q}-\frac{1}{\sigma_0\tau_3} \tag{4}$$

and $S>0$. Hence, the emitted intensity $P=S\tilde{c}wE_{phot}N_p$ (where w is the ridge dimension, E_{phot} the photon energy, and N_p the number of the periods in the active region) decreases linearly with a linear increase of $1/\tau_3$. In Eqs. (3) and (4), only $1/\tau_3$ is expected to vary significantly with B. Thus, the magnetic field dependance of the emitted power is a powerful tool to investigate the scattering mechanisms in QCLs. To reproduce the experimental oscillations, it is meaningful to calculate the scattering rate versus B for an electron in the $p=0$ Landau level of the third subband.

In Fig. 5(b), we compare the emitted power of the QCL, measured at a constant injected current of $I=1.42$ A (solid line), with the calculated $-1/\tau_3$ as a function of B. The scattering rate is calculated by using the model described in Ref. 15 with $\delta=6$ meV. The $1/\tau_3$ curve includes the contribution of the first 90 Landau levels. The most important contribution to the total scattering rate comes from transitions with final states $n=2$ and $n=1$. The plot of $-1/\tau_3(1/\tau_3=1/\tau_{31}+1/\tau_{32})$ as a function of B is shown by a dashed line. The curve has the same behavior as the experimental one; the minima of $-1/\tau_3$ correspond to the magnetophonon resonance condition [Fig. 5(a) (circles)]. The dashed-dotted line shows the total scattering rate when the number of final states is increased by adding contributions from scattering by LO phonons to the injector states indicated by i_1, i_2, and i_3 in Fig. 1. The two theoretical curves display the same behavior and the peak positions are not modified by the increased number of final states. The only difference is in the relative amplitude of the oscillations, which also slightly affects the peak width. The inclusion of the injector states in the calculation of the total scattering rate $1/\tau_3$ improves the agreement between the experimental and the calculated curves of the emitted power as a function of B.

It is worth noting that the general trend of the experimental curves is relatively well reproduced by the theory. Nevertheless, some of the experimental features are completely missing [like the peak at 18 T indicated by a vertical arrow in Fig. 5(b)]. In order to check if there are further contributions to the total scattering rate $1/\tau_3$, we performed a Fourier transform of both experimental and theoretical data to extract the characteristic frequencies of the oscillations.[1] This is justified by the fact that the scattering rate is quasiperiodic with the reciprocal magnetic field $1/B$, as we can see from the magnetophonon resonance condition, Eq. (2). The Fourier transform of the calculated total scattering rate $1/\tau_3$ as a function of $1/B$ is presented in Fig. 6 (dashed line). The curve exhibits two peaks which originate from two oscillating series associated with the scattering from $|3,0\rangle$ to $|2,p\rangle$ and $|1,p\rangle$.[19] In the same way, we perform the Fourier transform of $-P$ as a function of $1/B$, as extracted from the experimental curve shown in Fig. 5 (solid line). The experimental curve presents three peaks: two of them are in very good agreement with the theoretical ones and correspond to the energies $E_3-E_2-\hbar\omega_{LO}=75$ meV and $E_3-E_1-\hbar\omega_{LO}=111$ meV (obtained with an effective mass of $0.08m_0$, estimated by taking into account band nonparabolicity). The third peak corresponds to an energy of ≈ 150 meV, which fits very well with the transition energy E_3-E_1. Therefore, this third oscillating series is due to an elastic scattering from $|3,0\rangle$ to the states $|1,p\rangle$ $(p>0)$, as shown in Fig. 5. The elastic series due to the scattering from $|3,0\rangle$ to $|2,p\rangle$ does not give rise to an extra peak in the Fourier transform, because the active region is engineered such that $E_2=E_1+\hbar\omega_{LO}$; therefore, this series oscillates at the same frequency as the magnetophonon one. The presence of magneto-oscillations corresponding to elastic scattering and LO-phonon emission have already been observed in magnetotunneling experiments on GaAs/Al(Ga)As double barrier diodes.[20,21]

In the following we shall investigate which are the possible physical mechanisms providing the elastic scattering.

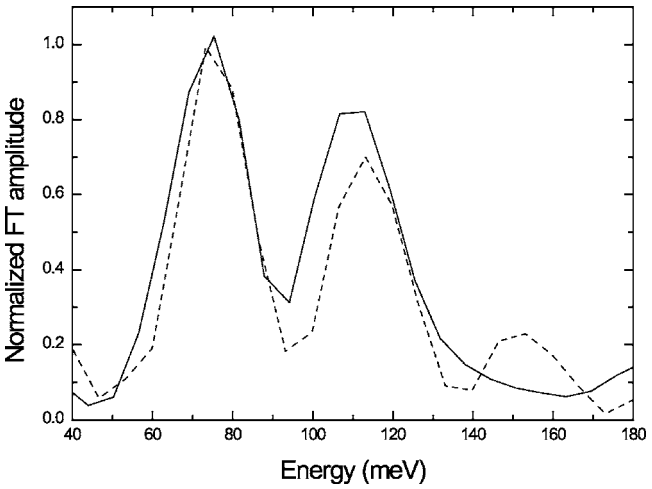

FIG. 6. Normalized amplitude of the Fourier transform of experimental $-P$ vs $1/B$ (solid line) and calculated $1/\tau_3$ vs $1/B$ (dashed line) as a function of their position in energy. The scattering time is obtained by taking into account only LO-phonon scattering. Note the high field peak arising from the elastic scattering contribution.

The contribution of several mechanisms to the scattering rate will be calculated at low temperatures: interface roughness, longitudinal acoustic (LA) phonon emission, impurity, and alloy scattering. We will show that in the case of the present active region, the interface roughness scattering turns out to be the most efficient mechanism responsible for the extra peak observed in the Fourier transform of the experimental data.

C. Interface roughness scattering

Several authors pointed out that interface roughness might contain two or more different length scales.[22] In particular, Warwick and Kopf[23] showed that the luminescence properties of a single GaAs/AlGaAs quantum well are affected by a "bimodal" interfacial roughness: substantial roughness on length scales greater than the exciton diameter and microroughness at length scales shorter than the exciton diameter. This bimodal behavior was confirmed by de Oliveira *et al.*,[24] by studying the relation between the interface microroughness and the full width at half maximum of the photoluminescence (PL) spectra for a GaAs/AlGaAs multiquantum well system.

In our model, we also assume that, in addition to the inhomogeneous broadening of the Landau levels, the interface roughness, at a smaller scale than the lateral extent of μ samples, is responsible of a homogeneous broadening. Following Ando[25] and many authors (see Ref. 22 for a review), we assume that the roughness height at the in-plane position $\mathbf{r}=(x,y)$ has a Gaussian correlation function:[26]

$$\langle \Delta(\mathbf{r})\Delta(\mathbf{r}')\rangle = \Delta^2 \exp\left(-\frac{|\mathbf{r}-\mathbf{r}'|^2}{\Lambda^2}\right), \tag{5}$$

where Δ is the mean height of the roughness and Λ the correlation length.

In a single quantum well, for a roughness located at the interface L_I, the scattering matrix element is given by

$$\langle m\mathbf{k}'|H_{IR}|n\mathbf{k}\rangle = \int d^2 r F_{mn}\Delta(\mathbf{r})e^{i(\mathbf{k}-\mathbf{k}')\cdot\mathbf{r}} \tag{6}$$

with

$$F_{mn} = V_0 \chi_m^*(L_I)\chi_n(L_I), \tag{7}$$

where χ_n is the z component of the wave function of the nth subband and V_0 is the barrier height. Let us stress that for fixed values of Δ and Λ, the scattering matrix element depends on the value of the wave function at the interfaces and, therefore, on n. The scattering matrix element is greater if the initial and final states are excited states, because their wave functions are less localized in the quantum well and have a greater value at the interfaces. As we can infer from Fig. 1, the active region of the QCL extends over three quantum wells and the $n=3$ wave function is non-negligible on at least six interfaces. Hence, it is very likely that the interface roughness contribution from subband $n=3$ to $n=1$ and $n=2$ of the QCL active region is non-negligible.

The active region of the present QCL contains several interfaces that are formed between barriers and wells of different widths. As we do not know the actual distribution of the roughness on each interface, we shall assume that each GaAs/AlGaAs interface of the active region presents the same correlation function and that there is no correlation between the roughness of different interfaces. We first calculate the interface roughness scattering rate as a function of the magnetic field, considering the mean height of the roughness Δ and the correlation length Λ as free parameters.

The calculation of the electron scattering rate due to the interface roughness in the presence of a magnetic field is performed in the same way as for LO phonons.[15] We evaluate the scattering rate in each of the N μ samples, which are characterized by thicknesses L randomly distributed. Then, we calculate the mean value of the scattering rate by integrating over L and assuming a Gaussian distribution $\Pi(L)$ for the thicknesses

$$\Pi(L) = \frac{1}{\sigma\sqrt{2\pi}}\exp\left(-\frac{(L-L_0)^2}{2\sigma^2}\right). \tag{8}$$

For an initial state $|3,0,0\rangle$, the scattering rate to a final state $|n,p,k_y\rangle$ is given by

$$\left\langle \frac{1}{\tau_{3,n}} \right\rangle = \frac{2\pi}{\hbar}\sum_{k_y,p} |\langle 3,0,0|\hat{H}_{IR}|n,p,k_y\rangle|^2 \times \int_{-\infty}^{+\infty} \Pi(L)\,\delta(\Delta_{3,n}(L) - p\hbar\omega_c)dL, \tag{9}$$

where $\hat{H}_{IR}$ is given by Eq. (6) (with the roughness located at an interface L_I of the active region) and $\Delta_{3,n}(L)=E_3(L)-E_n(L)$. Like in the work of Becker *et al.*,[15] we assume that around a mean value L_0, the energy difference $\Delta_{3,n}$ varies linearly with L

$$\Delta_{3,n}(L) = \Delta_{3,n}(L_0) - \gamma(L - L_0). \tag{10}$$

This results in a Gaussian distribution of the energy differences $\Delta_{3,n}$, characterized by a width $\delta = \gamma\sigma$. In the following, we will take $\delta = 6$ meV.

In order to calculate the scattering matrix element, we first average over the different roughness distributions; then we Fourier transform x and y components of the correlation function Eq. (5) to obtain

$$\left\langle \frac{1}{\tau_{3,n}}(L_I) \right\rangle = K(L_I) \sum_p \frac{l_c^{2p}}{2^p(\Lambda^2/4 + l_c^2/2)^{p+1}} \times e^{-(E_3 - E_n - p\hbar\omega_c)^2/(2\delta^2)},$$

$$K(L_I) = \frac{\pi}{\hbar} \frac{1}{\delta\sqrt{2\pi}} (F_{3n}\Lambda\Delta)^2, \tag{11}$$

where $l_c = \sqrt{\hbar/eB}$ is the magnetic length.

The total interface roughness scattering rate is obtained by adding the contribution of all the interfaces L_I of the active region

$$\frac{1}{\tau_{3n}} = \sum_{L_I} \left\langle \frac{1}{\tau_{3,n}}(L_I) \right\rangle. \tag{12}$$

We choose $\Lambda = 60$ Å and $\Delta = 1.5$ Å in order to have the best agreement between theoretical results on the total scattering rate and experimental data. These values are consistent with those found in the literature concerning GaAs/AlGaAs interfaces.[26–28] Since the correlation function is an assumption of the model, we have also checked that we obtain the same order of magnitude for the scattering rate with a different shape of this function (an exponential instead of a Gaussian).

Figure 7 shows that, as expected, the inclusion of the interface roughness scattering in the calculation of $1/\tau_3$ explains the existence of the missing peak at 18 T. Moreover, the inclusion of this further oscillating series gives an extra peak in the Fourier transform amplitude at the same frequency as observed experimentally. From Fig. 7, we can also see that whenever LO-phonon emission is inhibited, interface roughness (IR) scattering becomes an important relaxation mechanism. In the following we compare it to other elastic relaxation channels and show that the interface roughness scattering is the dominant scattering mechanism whenever LO-phonon emission is inhibited. Moreover, even at $B = 0$ T, when the LO-phonon emission is very efficient, the interface roughness scattering is not a negligible mechanism in our QCL structure due to the sizeable value of the wave functions at interfaces: at $B = 0$ $1/\tau_3^{(\mathrm{LO})} = 0.8$ ps^{-1} and $1/\tau_3^{(\mathrm{IR})} = 0.4$ ps^{-1}. As a consequence, we expect the interface roughness to considerably affect the performances of the QCL, as will be discussed in the following.

D. Contribution of other elastic or quasielastic scattering mechanisms

In this section, we will compare the interface roughness scattering to other relaxation mechanisms involving electrons on the excited $n = 3$ level of the laser transition: LA-phonon emission, impurity, and alloy scattering. We will evaluate them at $B = 0$ T and show that at low temperature, they are all negligible with respect to the interface roughness scattering. As their dependence on B is the same as for the interface roughness scattering, they will not be taken into account in the calculation of the scattering rates as a function of the magnetic field. We will finally discuss the effect of electron-electron interaction on the calculation of the scattering rates and the reason why we will neglect this relaxation channel in our calculations.

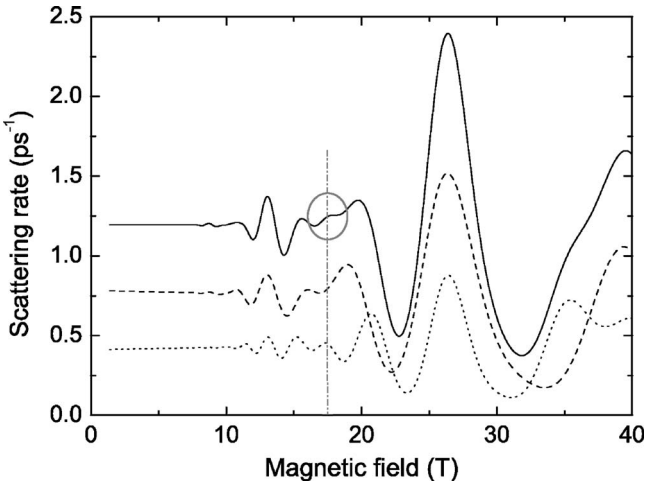

FIG. 7. Interface roughness (dotted line), LO-phonon (dashed line), and total (solid line) scattering rates as a function of the magnetic field. Interface roughness produces the peak at 18 T.

We calculated electron-LA-phonon interaction within the deformation potential approximation[29] by considering isotropic acoustical branches (sound velocity c_s). At low temperature, the scattering rate from state $|n=3, k_i=0\rangle$ to $|n, k_f\rangle$ by the emission of one LA phonon is given by

$$\frac{1}{\tau} = \frac{c_0}{\pi\hbar} \int_{-\infty}^{+\infty} dq_\parallel |f(q_\parallel)|^2 \int_0^{+\infty} dQ\, Q\hbar c_s \sqrt{q_\parallel^2 + Q^2} \times \delta\left(E_3 - E_n - \hbar c_s \sqrt{q_\parallel^2 + Q^2} - \frac{\hbar^2}{2m^*} Q^2 \right), \tag{13}$$

where $(q_\parallel, \vec{Q})$ is the wave vector of the emitted LA phonon, $f(q_\parallel) = \int_{-\infty}^{+\infty} dz\, e^{iq_\parallel z} \chi_i(z)\chi_f(z)$, $c_0 = D^2/2\rho c_s^2$ and D is the deformation potential for electrons. LA phonons between 0 and 3.5 meV are taken into account, resulting in a scattering rate from $n = 3$ to $n = 2$ subband of 0.01 ps^{-1}, which is twenty times smaller than the one obtained by the interface roughness scattering at $B = 0$ T.

In order to prevent space-charge formation, the injector of QCLs is doped.[18] As a consequence, ionized impurities are present close to but not in the active region, as shown by the shaded region in Fig. 1. The scattering by ionized impurities for an electron on the $n = 3$ subband is calculated following Ferreira and Bastard.[29] The scattering rate is given by

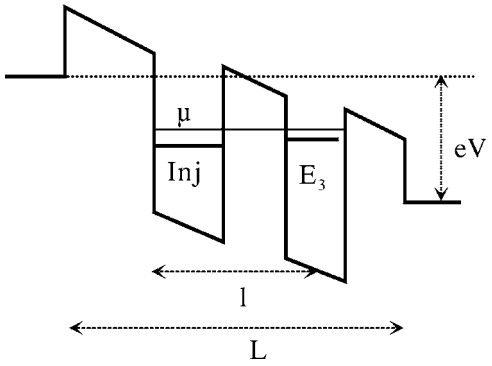

FIG. 8. Schematization of the system constituted by the active region and the injector as a double barrier subjected to an electric field F.

$$\frac{\hbar}{2\tau_{3n}} = \left(\frac{e^2}{4\varepsilon_0\kappa}\right)^2 N_{imp} \sum_{n,E_n<E_3} \frac{1}{E_3 - E_n} \times |\langle \chi_n | e^{-|z-z_i|\sqrt{2m^*(E_3-E_n)/\hbar^2}} | \chi_3 \rangle|^2, \quad (14)$$

where N_{imp} is the areal concentration of impurities (in our case $N_{imp}=2\times10^{11}$ cm^{-2}), z_i is the location of impurities, ε_0 is the permittivity of the vacuum, and κ the relative dielectric constant. Since in our case, the impurities are located far from the wells where the wave function $n=3$ is confined, this ionized impurity mechanism is much less efficient than the interface roughness; the calculated relaxation rate (with final state $n=2$) is $1/\tau_{32} \simeq 4\times10^{-6}$ ps^{-1}.

We also evaluated the effect of alloy scattering due to AlGaAs barriers.[26,28,30] Since in the present structure the alloy disorder is only present in the barriers and not in the wells, the alloy scattering is expected to be a small effect. For a transition between $n=3$ and $n=2$ subband, we found a scattering rate of 0.1 ps^{-1}, which is still negligible with respect to the interface roughness.

Electron-electron scattering has proved to be important for sufficiently high carrier densities and even to be the dominant mechanism of intersubband carrier relaxation in QCLs designed to emit in the THz frequency range. Typical electron densities for the $n=3$ subband in our system are of the order of 2×10^{10} cm^{-2} (evaluated by considering $n_3 = J_{th}\times\tau_3/e$), which is greater than the typical electron densities[6] involved in a THz QCL. As a consequence, the simple value of the electron density does not allow us to neglect electron-electron scattering in our calculation. A more detailed analysis needs to be done. Kempa *et al.*[31] showed that the behavior of the scattering rate as a function of the applied magnetic field allows one to distinguish between two-electron and one-electron processes because they lead to different energy conservation relations. In particular, for two electrons going from the upper $|3,0\rangle$ Landau level to two different Landau levels p and m of the second subband, the energy conservation condition leads to[31]

$$E_3 - E_2 = \frac{\hbar\omega_c}{2}(p+m). \quad (15)$$

In this case, the scattering rate as a function of B presents further peaks with respect to those obtained with a one-electron calculation, due to the contribution of all processes with an odd value of $p+m$. These peaks, already observed in the case[6] of a THz QCL, are not observed in our system. Another possible two-electron process is the one in which only one electron changes the subband. The scattering rate due to this mechanism oscillates with respect to B with the same peaks as the elastic scattering discussed in this paragraph. Anyway, its amplitude should depend on the electron density of the $|3,0\rangle$ Landau level;[32] as a consequence, it should lead to a variation of the relative amplitude for the elastic and inelastic oscillations with respect to the injected current. This variation has not been observed in our structure. As we did not find any evidence for electron-electron scattering in our structure, we neglect this contribution in the calculation of the total scattering rate.

TABLE I. Comparison between the different scattering processes for an electron on the $n=3$ subband at $B=0$. Lifetimes are presented for $3\rightarrow2$ transition (τ_{32}) and for the total scattering time (τ_3).

Scattering mechanism	τ_{32}(ps)	τ_3(ps)
LO phonons	2.9	1.3
Interface roughness	5.26	2.5
LA phonons	100	60.6
Impurities	2.8×10^5	1.9×10^5
Alloy scattering	9.6	5.6

A summary of the calculated scattering rates is presented in the Table I.

V. ABOVE AND BELOW THRESHOLD BEHAVIOR

Measurements of the emitted laser intensity as a function of the magnetic field show in an impressive way how the different scattering mechanisms affect the electron lifetime. Nevertheless, these kinds of measurements only give access to the QCL's behavior above threshold. On the other hand, oscillations of the electron lifetime with the magnetic field also affect transport measurements, in particular below threshold.

We have already shown in Fig. 4(b), the oscillations of $V(B)$ at constant current. In order to understand these oscillations, let us consider a simple model for our system. Below threshold [$S=0$ in the rate equation system (3)], the population in the upper level of the laser transition is given by

$$\eta\frac{J}{q} = \frac{n_3}{\tau_3}. \quad (16)$$

As the injection current is constant with B, n_3 depends only on τ_3. The system constituted by the active region and the injector can roughly be considered as a double well in equilibrium between two highly charged layers with a common quasi-Fermi level μ spanning the injector and the active region,[33] as is schematically shown in Fig. 8. If we suppose that the population n_3 does not affect the band profile, we can write that $n_3=(m^*/\pi\hbar^2)[\mu-E_3(F)]$, where F is the electric field applied to the structure. If L is the total length of a

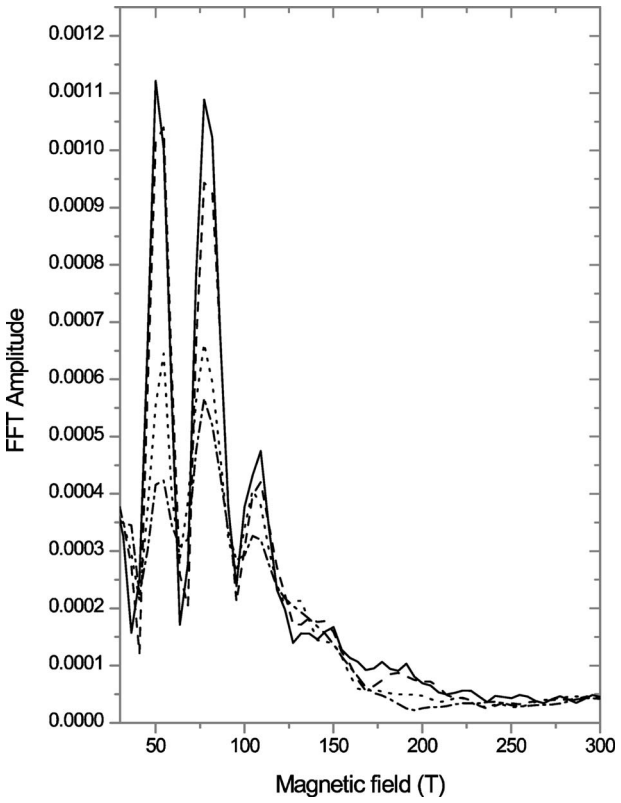

FIG. 9. Fourier transform of $1/V$ vs $1/B$ for the following current values: 0.842 I_{th} (solid line), 0.942 I_{th} (dashed line), 1.04 I_{th} (dotted line), 1.15 I_{th} (dashed-dotted line). Three peaks are observed as in the Fourier transform of $-P$ vs $1/B$, corresponding to LO-phonon emission and elastic scattering.

period and l is the distance between the injector and the quantum well where the optical transition takes place, $\mu - E_3 \propto eVl/L$, and hence, $n_3 \propto V$. As a consequence, the oscillatory part of the measured voltage varies with the magnetic field proportionally to τ_3.

Above threshold, the relationship between the current density and the scattering rate has to be rewritten by taking into account the stimulated emission rate, $1/\tau_{st} = \sigma_0 S$. After introducing $1/\tau_{st}$ into the rate equations (3), we find

$$\eta \frac{J}{q} = n_3 \left(\frac{1}{\tau_3} + \frac{1}{\tau_{st}} \right), \tag{17}$$

where J is constant with respect to the magnetic field. This means that below threshold, the oscillations of the measured voltage are directly related to the scattering rate; on the contrary, above threshold they are due to both variations of $1/\tau_3$ and $1/\tau_{st}$ as functions of B. As $1/\tau_{st}$ is proportional to the emitted power, it oscillates like $-1/\tau_3$ with the applied magnetic field. As a consequence, when the two terms are comparable in intensity (like when the device is just above threshold) they compensate each other and the oscillations are almost suppressed. In the inset of Fig. 4(b), we see indeed that oscillations are less pronounced above threshold. This effect is also evident in the Fourier transforms of $1/V$ versus $1/B$, as shown in Fig. 9. We can see that, as $I/I_{th} > 1$, the peak amplitude decreases considerably.

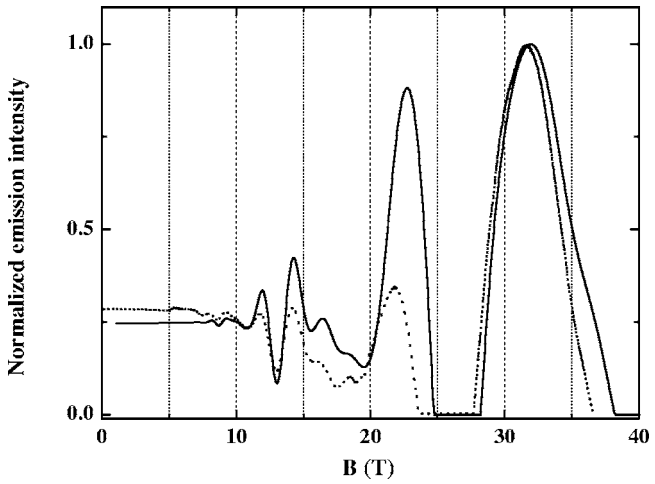

FIG. 10. Comparison between the calculated (solid line) and experimental (dotted line) laser emission.

VI. CONCLUSION

In conclusion, we have shown that the magnetic field is an efficient spectroscopic tool to ascertain the nature and magnitude of the scattering mechanisms in the active region of a QCL. We have presented a detailed experimental and theoretical study of a GaAs/AlGaAs QCL under strong magnetic field at low temperature.

In particular, we have studied the oscillations of the emitted power as a function of B. By a detailed analysis of the oscillations, we have found that the elastic scattering is a non-negligible relaxation mechanism for electrons on the excited state of the laser transition. We have calculated the contribution of several elastic scattering mechanisms, showing that, at low temperature, the interface roughness is the dominant one for this structure. By comparing experimental and numerical results, we have deduced typical parameters of the interface roughness correlation function. By using a simplified rate equation system [Eq. (3)], we have calculated the emitted power as a function of the magnetic field. The result is shown in Fig. 10: all the experimental peaks are very well reproduced. The differences in the relative amplitude of the peaks are probably due to the energy positions of the injector states, which cannot be deduced from luminescence measurements.

It is worth noting that by interpolating our numerical results to $B=0$ T, we find that elastic relaxation is an efficient scattering mechanism at low temperature in the case of a GaAs/AlGaAs QCL. This information may be helpful in order to understand which are the most important relaxation paths for electrons electrically injected in the active region of the QCL. The problem of the relaxation of carriers in the active region is not only a fundamental question, but also a technological one: nowadays, heat dissipation is the most important limitation to QCLs performances.

ACKNOWLEDGMENTS

We wish to acknowledge useful discussions with Clément Faugeras. We gratefully acknowledge the financial support of

EU FP6 Grant No. STRP505642 "ANSWER" and support from NHMFL In House Research Program (Project No. 5053). The NHMFL is supported by NSF Cooperative Agreement No. DMR-0084173, by the State of Florida, and by the DOE. The LPA-ENS is "laboratoire associé au CNRS et aux Universités Paris 6 et Paris 7."

*Corresponding author. Electronic address: Angela.Vasanelli@thalesgroup.com

[1] C. Becker, C. Sirtori, O. Drachenko, V. Rylkov, D. Smirnov, and J. Leotin, Appl. Phys. Lett. **81**, 2941 (2002).
[2] D. Smirnov, C. Becker, O. Drachenko, V. V. Rylkov, H. Page, J. Leotin, and C. Sirtori, Phys. Rev. B **66**, 121305(R) (2002).
[3] D. Smirnov, O. Drachenko, J. Leotin, H. Page, C. Becker, C. Sirtori, V. Apalkov, and T. Chakraborty, Phys. Rev. B **66**, 125317 (2002).
[4] S. Blaser, M. Rochat, M. Beck, D. Hofstetter, and J. Faist, Appl. Phys. Lett. **81**, 67 (2002).
[5] V. Tamosiunas, R. Zobl, J. Ulrich, K. Unterrainer, R. Colombelli, C. Gmachl, K. West, and L. Pfeiffer, Appl. Phys. Lett. **83**, 3873 (2003).
[6] G. Scalari, S. Blaser, J. Faist, H. Beere, E. Linfield, D. Ritchie, and G. Davies, Phys. Rev. Lett. **93**, 237403 (2004).
[7] J. Alton, S. Barbieri, J. Fowler, H. E. Beere, J. Muscat, E. H. Linfield, D. A. Ritchie, G. Davis, R. Köhler, and A. Tredicucci, Phys. Rev. B **68**, 081303(R) (2003).
[8] G. Scalari, S. Blaser, L. Ajili, J. Faist, H. Beere, E. H. Linfeld, D. A. Ritchie, and G. Davies, Appl. Phys. Lett. **83**, 3453 (2003).
[9] J. Radovanović, V. Milanović, Z. Ikonić, D. Indjin, and P. Harrison, J. Appl. Phys. **97**, 103109 (2005).
[10] V. M. Apalkov and T. Chakraborty, Appl. Phys. Lett. **78**, 697 (2001).
[11] S. Blaser, L. Diehl, M. Beck, and J. Faist, Physica E (Amsterdam) **7**, 33 (2000).
[12] P. Kruck, H. Page, C. Sirtori, S. Barbieri, M. Stellmacher, and J. Nagle, Appl. Phys. Lett. **76**, 3340 (2000).
[13] C. Sirtori, F. Capasso, J. Faist, and S. Scandolo, Phys. Rev. B **50**, 8663 (1994).
[14] U. Ekenberg, Phys. Rev. B **40**, 7714 (1989).
[15] C. Becker, A. Vasanelli, C. Sirtori, and G. Bastard, Phys. Rev. B **69**, 115328 (2004).
[16] C. Weisbuch, R. Dingle, A. C. Gossard, and W. Wiegmann, Solid State Commun. **38**, 709 (1981).
[17] In the picture, the level $\varepsilon_{3,0}-\hbar\omega_{LO}$ is represented in order to evidence at the same time magnetophonon resonances as well as elastic transitions. Physically, one LO-phonon replica from $|2,p\rangle$ and $|1,p\rangle$ cross the zero phonon $|3,0\rangle$ level.
[18] J. Faist, F. Capasso, C. Sirtori, D. L. Sivco, and A. Y. Cho, in *Intersubband Transitions in Quantum Wells: Physics and Device Applications II*, Semiconductors and Semimetals Vol. 66 (Academic Press, San Diego, 2000).
[19] The two Fourier transforms have been calculated over the same interval in $1/B$; as a consequence, they have the same resolution. For this reason, the peaks relative to transitions from $|3,0\rangle$ to the injector states i_1, i_2, i_3 are not resolved in the theoretical curve.
[20] Y. G. Gobato, F. Chevoir, J. M. Berroir, P. Bois, Y. Guldner, J. Nagle, J. P. Vieren, and B. Vinter, Phys. Rev. B **43**, 4843 (1991).
[21] G. S. Boebinger, A. F. J. Levi, S. Schmitt-Rink, A. Passner, L. N. Pfeiffer, and K. W. West, Phys. Rev. Lett. **65**, 235 (1990).
[22] E. Runge, Solid State Phys. **57**, 149 (2002).
[23] C. A. Warwick and R. F. Kopf, Appl. Phys. Lett. **60**, 386 (1992).
[24] J. B. B. de Oliveira, E. A. Meneses, and E. C. F. da Silva, Phys. Rev. B **60**, 1519 (1999).
[25] T. Ando, A. B. Fowler, and F. Stern, Rev. Mod. Phys. **54**, 437 (1982).
[26] T. Unuma, M. Yoshita, T. Noda, H. Sakaki, and H. Akiyama, J. Appl. Phys. **93**, 1586 (2003), and references therein.
[27] T. Unuma, T. Takahashi, T. Noda, M. Yoshita, H. Sakaki, M. Baba, and H. Akiyama, Appl. Phys. Lett. **78**, 3448 (2001).
[28] F. Chevoir and B. Vinter, Phys. Rev. B **47**, 7260 (1993).
[29] R. Ferreira, and G. Bastard, Phys. Rev. B **40**, 1074 (1989).
[30] T. Ando, J. Phys. Soc. Jpn. **51**, 3900 (1982).
[31] K. Kempa, Y. Zhou, J. R. Engelbrecht, P. Bakshi, H. I. Ha, J. Moser, M. J. Naughton, J. Ulrich, G. Strasser, E. Gornik, and K. Unterrainer, Phys. Rev. Lett. **88**, 226803 (2002).
[32] K. Kempa, Y. Zhou, J. R. Engelbrecht, and P. Bakshi, Phys. Rev. B **68**, 085302 (2003).
[33] C. Sirtori, F. Capasso, J. Faist, A. L. Hutchinson, D. L. Sivco, and A. Y. Cho, IEEE J. Quantum Electron. **34**, 1722 (1998).